Diagnostic Accuracy of Quantitative Micro-Elastography for Margin Assessment in Breast-Conserving Surgery

Kelsey M. Kennedy[1], Renate Zilkens[1,2], Wes M. Allen[1,3], Ken Y. Foo[1,3], Qi Fang[1,3], Lixin Chin[1,3], Rowan W. Sanderson[1,3], James Anstie[1,3], Philip Wijesinghe[1,3], Andrea Curatolo[1,3], Hsern Ern I. Tan[2], Narelle Morin[4], Bindu Kunjuraman[5], Chris Yeomans[6], Synn Lynn Chin[5], Helen DeJong[1], Katharine Giles[7], Benjamin F. Dessauvagie[2,6], Bruce Latham[6], Christobel M. Saunders[2,5,8], and Brendan F. Kennedy[1,3]

ABSTRACT

Inadequate margins in breast-conserving surgery (BCS) are associated with an increased likelihood of local recurrence of breast cancer. Currently, approximately 20% of BCS patients require repeat surgery due to inadequate margins at the initial operation. Implementation of an accurate, intraoperative margin assessment tool may reduce this re-excision rate. This study determined, for the first time, the diagnostic accuracy of quantitative micro-elastography (QME), an optical coherence tomography (OCT)–based elastography technique that produces images of tissue microscale elasticity, for detecting tumor within 1 mm of the margins of BCS specimens. Simultaneous OCT and QME were performed on the margins of intact, freshly excised specimens from 83 patients undergoing BCS and on dissected specimens from 7 patients undergoing mastectomy. The resulting three-dimensional images ($45 \times 45 \times 1$ mm) were coregistered with postoperative histology to determine tissue types present in each scan. Data from 12 BCS patients and the 7 mastectomy patients served to build a set of images for reader training. One hundred and fifty-four subimages ($10 \times 10 \times 1$ mm) from the remaining 71 BCS patients were included in a blinded reader study, which resulted in 69.0% sensitivity and 79.0% specificity using OCT images, versus 92.9% sensitivity and 96.4% specificity using elasticity images. The quantitative nature of QME also facilitated development of an automated reader, which resulted in 100.0% sensitivity and 97.7% specificity. These results demonstrate high accuracy of QME for detecting tumor within 1 mm of the margin and the potential for this technique to improve outcomes in BCS.

Significance: An optical imaging technology probes breast tissue elasticity to provide accurate assessment of tumor margin involvement in breast-conserving surgery.

Introduction

Success of breast-conserving surgery (BCS) is characterized by clear margins and a good cosmetic outcome for the patient. However, approximately 20% of cases require repeat surgery due to inadequate margins (1–3). Re-excision surgery causes substantial physical, psychologic, and financial burdens for patients, with higher risk of complications (4), worse cosmesis, and additional costs, on average, of >$10,000 per patient (5). Intraoperative detection of tumor at the margins would allow more complete resection of malignant tissue in the first operation, provide the surgeon with confidence that no residual cancer remains in the breast, and reduce the number of re-excision surgeries.

Several techniques are currently used for intraoperative margin assessment. Intraoperative pathologic assessment can be performed using frozen section analysis and imprint cytology (6), but these techniques are resource-intensive, sample only a small percentage of the surgical margins, and have limited efficacy, especially for ductal carcinoma *in situ* (DCIS; ref. 7), and, thus, have not been widely adopted (8). Another available technique, intraoperative specimen radiography (IOSR), provides an X-ray image of the excised specimen. IOSR can show that the main lesion has been removed, which is particularly useful for nonpalpable tumors that are localized using preoperative wire insertion (9) or radioactive seed placement (10). However, IOSR accurately predicts margin status in only 48% of cases (11) and has been shown not to reduce re-excision rates (11, 12). Intraoperative ultrasound guidance of excision has been shown in a small number of studies to reduce re-excision rates by more than half for invasive cancers (13, 14), but ultrasound is operator-dependent and has limited reliability for visualizing *in situ* or multifocal cancers (15, 16).

To address the shortcomings of existing techniques, a range of margin assessment tools have been proposed, relying on various contrast mechanisms to detect cancer. One commercially available technique uses radiofrequency spectroscopy to measure the dielectric properties of tissue, implemented in a handheld probe (MarginProbe, Dune Medical Devices). The technique shows high accuracy for margin assessment in homogeneous, *ex vivo* tissues (e.g., if the probe is placed over a large region of tumor, >6 mm diameter) but has lower accuracy (70% sensitivity and 70% specificity) when multiple tissue

[1]BRITElab, Harry Perkins Institute of Medical Research, QEII Medical Centre, Nedlands, and Centre for Medical Research, The University of Western Australia, Perth, Australia. [2]School of Medicine, The University of Western Australia, Perth, Australia. [3]Department of Electrical, Electronic & Computer Engineering, School of Engineering, The University of Western Australia, Perth, Australia. [4]Sonowest, Perth, Australia. [5]Breast Centre, Fiona Stanley Hospital, Murdoch, Australia. [6]PathWest, Fiona Stanley Hospital, Murdoch, Australia. [7]OncoRes Medical, Perth, Australia. [8]Breast Clinic, Royal Perth Hospital, Perth, Australia.

Note: Supplementary data for this article are available at Cancer Research Online (http://cancerres.aacrjournals.org/).

Current address for K.M. Kennedy: Department of Biomedical Engineering, Columbia University, New York, NY; current address for P. Wijesinghe, School of Physics and Astronomy, University of St. Andrews, United Kingdom; and current address for A. Curatolo: VioBio, Instituto de Óptica "Daza de Valdés", Consejo Superior de Investigaciones Cientificas (IO, CSIC), Madrid, Spain.

Corresponding Author: Brendan F. Kennedy, The University of Western Australia, 35 Stirling Highway, Perth, Western Australia 6009, Australia. Phone: 618-6488-4746; Fax: 618-6488-1319; E-mail: brendan.kennedy@uwa.edu.au

Cancer Res 2020;80:1773–83

doi: 10.1158/0008-5472.CAN-19-1240

types are present in the interrogated region (17). In a randomized trial with 596 patients, use of MarginProbe on excised specimens reduced re-excision rate from 25.8% to 19.8% but suffered from low specificity with a 53.6% false positive rate (18).

Fluorescent modalities that utilize molecular contrast to intraoperatively highlight cancer are also under development, potentially enabling surgeons to visualize tumor in the cavity, as well as in the excised lump (19–22). A small number of proof-of-principle studies in humans have been reported (19, 20, 22), but the efficacy of these techniques for reducing re-excision rates in BCS has not been determined. In addition, they typically rely on preoperative, systemic administration of exogenous dyes, requiring extensive dosing and tumor uptake studies, and creating potential barriers to clinical translation (19). Another optical technique, surface-enhanced Raman scattering (23), has recently been proposed, using targeted nanoparticles for multiplexed imaging of cancer biomarkers. A preliminary study on *ex vivo* tissues dissected from mastectomy and lumpectomy specimens showed promising sensitivity (89.3%) and specificity (92.1%) for cancer detection, and the technique is conducive to personalized biomarker imaging based on tumor-specific molecular profiles. However, it is restricted to surface imaging, and, while many institutions have adopted a "no tumor on ink" criterion for invasive cancers, larger margins are typically desired for *in situ* cancers (1). Label-free optical techniques have also been proposed, including diffuse reflectance spectroscopy/hyperspectral imaging (24, 25), autofluorescence lifetime imaging, and Raman spectroscopy (26). However, diffuse techniques can suffer from low spatial resolution (~5 mm; ref. 24), while autofluorescence and Raman techniques typically have low scanning speeds (12–24 minutes/margin; ref. 26), making clinical translation more challenging.

Optical coherence tomography (OCT) is a promising optical technique capable of three-dimensional (3D), high-speed, high-resolution imaging without need for exogenous contrast agents. OCT may be described as an optical analogue to ultrasound. It uses interferometry to effectively measure "time of flight" of light in tissue, creating an image based on the amount of back-scattered light, with microscopic resolution (2–10 μm) up to 1 to 2 mm in depth. These imaging specifications match well with the clinical requirements of margin assessment in BCS. Preliminary studies have reported high sensitivity (80–94%) and specificity (87–93%) for detecting cancer, primarily in mastectomy tissues (27–29). However, these mastectomy samples were typically dissected to expose a bulk of dense, high-grade tumor for imaging. The image contrast in this scenario may not translate to margin assessment in BCS, in which typically lower-grade tumors must be detected at the edge of intact specimens or, for detecting residual tumor, directly within the surgical cavity. The largest study to date that used OCT to assess margins in BCS specimens reported sensitivity of 55% to 65% and specificity of 68% to 70% (30). One reason for this relatively low accuracy may be the limited ability of OCT to distinguish between tumor and surrounding normal stroma (31–33). Stronger contrast between tissue types is expected to aid surgeon decision-making in the intraoperative setting (34, 35).

Beyond its distinct molecular and optical properties, breast cancer also exhibits distinct mechanical properties (36–38). At the cellular scale, atomic force microscopy has revealed unique mechanical signatures within the breast tumor microenvironment caused by the mix of cellular proliferation and desmoplastic stroma (37). At the macroscale, surgeons rely on mechanical changes as they manually palpate the tissue, feeling for the boundaries of the typically stiff lesion. However, palpation is a subjective tool, and a large proportion of breast lesions are considered "impalpable," that is, too small or soft to detect through touch (39). Elastography is a technique that creates images of the mechanical properties of tissue, complementing palpation by visualizing mechanical changes in 2D or 3D. Elastography based on ultrasound has been developed for a number of applications, including preoperative diagnosis of breast lesions (38, 40), but has not been applied to intraoperative margin assessment, mainly due to its relatively low spatial resolution (see Supplementary Information, "Note on elastography of the breast.") In an emerging technique, OCT elastography is used to measure tissue deformation under an applied load, offering 3D maps of mechanical properties with microscale resolution (41). OCT elastography techniques can be classified according to the mechanical loading mechanism used, with compression and shear wave being the most prominent (41). Although early compression OCT elastography studies produced maps of tissue deformation (strain; refs. 31, 42), which is an indirect and qualitative measure of elasticity, introduction of a stress sensing technique to map the local stress in 2D at the tissue surface, has enabled quantitative micro-elastography (QME), providing 3D maps of local elasticity, under the assumption of uniaxial stress (43). Preliminary QME data in mastectomy specimens showed that elasticity images provide additional contrast between tumor and normal tissue compared to OCT and strain, and the technique has been extended to incorporate a wide-field scanning mechanism that enables entire margins of BCS specimens to be imaged within an intraoperative timeframe (44). To build on these promising feasibility studies and to determine the clinical potential of QME for intraoperative margin assessment, it must be established whether clinicians can interpret QME images to accurately identify close or positive tumor margins in BCS specimens. To this end, the goal of this study is to conduct, for the first time, a blinded reader study, with postoperative histology as the gold standard, to determine the diagnostic accuracy (sensitivity and specificity) of QME, compared with OCT alone, for detecting tumor within 1 mm of the margins of freshly excised specimens from patients undergoing BCS.

Patients and Methods

Patient recruitment and imaging

All study procedures were performed after approval by the ethics board of the South Metropolitan Area Health Service in Western Australia. Ninety patients were recruited for this study after informed written consent was obtained: 83 patients (with no prior excision) undergoing BCS for treatment of breast cancer and 7 patients undergoing mastectomy for treatment of breast cancer. Samples from the 7 mastectomy patients and 12 of the BCS patients were used to create a set of pilot data for training readers. Data from the remaining 71 BCS patients were included in the blinded reader study. **Table 1** summarizes the disease characteristics of all BCS patients. Supplementary Table S1 summarizes mastectomy patient characteristics.

For patients undergoing BCS, following surgery, the fresh, intact specimens were transferred to the pathology department at Fiona Stanley Hospital. Pathologists at this institution dictated that tissue should be placed in fixative (formalin) within 1 hour of receiving the specimen from surgery, to avoid any tissue degradation that might influence histological processing. Between excision and imaging, specimens were kept in air at room temperature, and the surface was kept hydrated by applying droplets of saline. Specimen orientation was maintained using clips and sutures, per standards at this institution. In most cases (8/12 pilot cases and 68/71 cases for the reader study), two margins were imaged. In the remaining cases, one margin was imaged due to delays in scanning the specimen within the allotted time. No more than two margins per specimen were scanned as, in addition to

Table 1. BCS patient and clinical specimen characteristics.

	Pilot study (12 patients)		Reader study (71 patients)	
Age, y	**Number**	**Percentage**	**Number**	**Percentage**
Mean	60		59	
SD	9		11	
Range	44–74		26–76	
≤65	8	67%	48	68%
>65	4	33%	23	32%
Surgical diagnosis[a]				
Ductal carcinoma *in situ*	6	50%	44	62%
Invasive ductal carcinoma	8	67%	43	61%
Invasive lobular carcinoma	2	17%	8	11%
Invasive mucinous carcinoma	1	8%	3	4%
Mixed invasive ductal lobular carcinoma	0	0%	2	3%
Invasive micropapillary carcinoma	0	0%	1	<1%
Invasive apocrine carcinoma	0	0%	1	<1%
Invasive solid papillary carcinoma	0	0%	2	3%
No tumor[b]	0	0%	3	4%
Palpability				
Palpable	7	58%	45	63%
Impalpable	5	42%	26	37%
Total lesion size (greatest dimension)				
<1 cm	1	8%	15	21%
1–2 cm	5	42%	27	38%
>2 cm	6	50%	26	37%
No tumor	0	0%	3	4%
Closest tumor margin[c]				
<1 mm[d]	7	58%	32	45%
1–3 mm	4	33%	25	35%
>3 mm	1	8%	11	15%
Not applicable (no tumor)	0	0%	3	4%

[a]Multiple tumor types may occur in a given patient, such that diagnosis percentages add to >100%.
[b]Tumor was excised in original core biopsy.
[c]Includes deep and superficial margins in addition to radial margins.
[d]Thirteen (18%) of BCS specimens in the reader study had positive margins (i.e., tumor on ink).

imaging, sufficient time was needed to transfer the specimen from pathology, select a margin for scanning and orientate the specimen in the imaging system. Margins for scanning were chosen based on consultation with pathologists, observation of the intraoperative specimen radiography (when available), and surgical notes indicating if extra cavity shavings were performed intraoperatively. The "closest tumor margin" distances reported in **Table 1** were determined by postoperative histology and include superficial and deep margins (considering radial margins only, which are most clinically relevant, the rate of tumor margins <1 mm in the reader study was 21%). For patients undergoing mastectomy, nondiagnostic tissue was dissected by a pathologist to create samples of approximately 5 × 5 × 0.5 cm, which were also imaged within approximately 1 hour of excision.

Imaging was performed on a benchtop, wide-field QME system as described previously (Supplementary Fig. S1A; ref. 44). Briefly, the system is based on a Telesto II spectral-domain OCT system (TEL220C1, Thorlabs). It uses a superluminescent diode light source with a central wavelength of 1300 nm and a bandwidth of >170 nm, illuminating the sample with 2.5 mW of power (a low power level that is safe for users). The measured axial and lateral resolutions in air are 5.5 μm and 13 μm, respectively. The system captures one-dimensional axial scans (A-scans) in 14 μs, and the beam is raster scanned to build a 3D image measuring 16 × 16 × 3.5 mm in 55 seconds. Wide-field images are generated by translating the specimen relative to the OCT scan head between 3D acquisitions, as described previously (42, 44). Nine subvolumes are acquired with 1-mm overlap in the lateral plane, resulting in a 45 × 45 × 3.5 mm image captured in under 9 minutes. The partially overlapping subvolumes are stitched to form mosaicked wide-field images, presented in the *en face* plane. The measured displacement sensitivity of the OCT system is 1.4 nm at an OCT signal-to-noise ratio of 40 dB, acquired under clinical testing conditions in the pathology laboratory (i.e., without a vibration isolation table).

A compliant silicone layer is placed between the specimen and imaging window to ensure contact between the uneven specimen surface and window, as well as to estimate stress for quantification of elasticity (43). After establishing contact, microscale displacement (up to 9.5 μm) was applied to the specimen surface using a piezoelectric actuator. Images were processed to determine stress, strain, and elasticity (Supplementary Fig. S1B), and elasticity was overlaid on the solid regions of the OCT images for visualization, using an algorithm described previously (42). OCT data are displayed in grayscale from 0 to 40 dB, and elasticity data are displayed in color on a logarithmic scale from 3.63 to 363 kPa.

Histopathology and coregistration with imaging data

Following imaging, specimens were fixed in formalin and submitted for standard histopathologic processing. Specimens were inked for orientation and sliced in "bread-loaf" fashion from lateral-to-medial, superficial-to-deep, or superior-to-inferior margins to generate histologic sections at each plane. This sectioning protocol resulted in histology typically being performed in a plane orthogonal to the *en face* plane in which QME images are displayed. The positions of the histology sections were coregistered with images by cross-referencing the blocking diagram and photographs taken of the specimen during scanning, as illustrated in Supplementary Fig. S2. Pathologists (BFD, BL) determined tissue types present in the histology images. Engineers and pathologists worked together to confirm coregistration by cross-checking tissue features present in the histology images with similar features present in the OCT images, using the depth cross-section (B-scan) view of OCT to match the histology plane where needed, as described in (42).

To focus the histologic analysis, and to facilitate the subsequent reader study, 3D regions of interest (ROI), 10 × 10 × 1 mm, were selected from the wide-field (45 × 45 × 1 mm) scans. At least one ROI was selected on every margin scanned in this study. ROIs were then included in the reader study if they met the following criteria: good physical contact with the specimen; tissue not extensively damaged by thermal effects (due to cauterization during resection) as assessed by histopathology; and availability of a reliable histology match for the ROI. Considering that histology slices are typically taken approximately every 3 mm, 1 to 3 sections were available for a given ROI. ROIs were designated as "positive" for cancer if the pathologist identified any tumor within 1 mm of the margin in the histology sections corresponding to the ROI, similar to designation of "positive" margins in other diagnostic accuracy studies in BCS specimens (26, 30). In each case, the ROI was selected before the histology was analyzed by the

pathologist. As such, the researchers selecting the ROI did not know the outcome of the corresponding histology. Note: The clinical standard at the hospital where the study was performed is 1 to 2 mm for invasive ductal carcinoma and 2 mm for DCIS.

Reader study and statistical analysis

The reader study was designed to have three main outcomes: diagnostic accuracy (sensitivity and specificity) of OCT, QME, and OCT plus QME. Seven readers [2 surgeons, 2 engineers, 1 medical sonographer, 1 pathology scientist (equivalent to a pathology assistant) and 1 medical resident], blinded to the histologic results, participated in the study. First, readers were trained to read OCT images in a 1.5-hour session. They then completed a reading of all ROIs (OCT alone, using criteria in **Fig. 1A**) within 10 days of training and had access to the training images during reading. Two weeks following the OCT training, readers were trained to read QME images in another 1.5-hour session. They then completed a reading of all ROIs once more, this time viewing OCT and QME side-by-side, from which accuracy was calculated for QME (using criterion in **Fig. 1B**) and OCT plus QME (using criterion in **Fig. 1C**). To remove potential bias due to reader memory, the order and orientation of ROIs were randomized between readings. In both readings, readers viewed the ROIs ($10 \times 10 \times 1$ mm, presented as a stack of *en face* images displayed every 20 μm up to 1 mm in depth) using the open source software ImageJ (v1.52a; ref. 45), which allowed scrolling through depth to visualize the volume. Readers completed their evaluation using a custom-built interface in which they followed a set of criteria for the presence of cancer in each image type and selected "cancer" or "not cancer" as the endpoint (**Fig. 1**).

Criteria for cancer in OCT images (**Fig. 1A**) were determined on the basis of three main observations from prior OCT studies of breast tissues (28, 32, 42, 46, 47) and pilot study data. First, it has been established that adipose tissue is easily distinguished from other tissues in breast based on its "honeycomb" structure in OCT. Therefore, readers were trained to first identify solid features >1 mm in diameter. If the ROI was made up of all adipose tissue or adipose tissue with only small (<1 mm), isolated solid features, it was considered "not cancer". Second, it was found in preliminary OCT studies on BCS specimens (42) and in this study that cancer near the margin tends to have continuity with depth, uninterrupted by regions of adipose tissue. Thus, if readers found a region of solid tissue, they were to scroll through the 3D image, checking if the feature extended down into the specimen. Finally, a criterion was added to help distinguish benign stroma from regions of cancer. In benign stroma, a striated or banded pattern is observed in OCT, likely due to the organization of the underlying collagen. Cancer tends to disrupt this organization and result in heterogeneous patterns in OCT (31, 48). One special case is

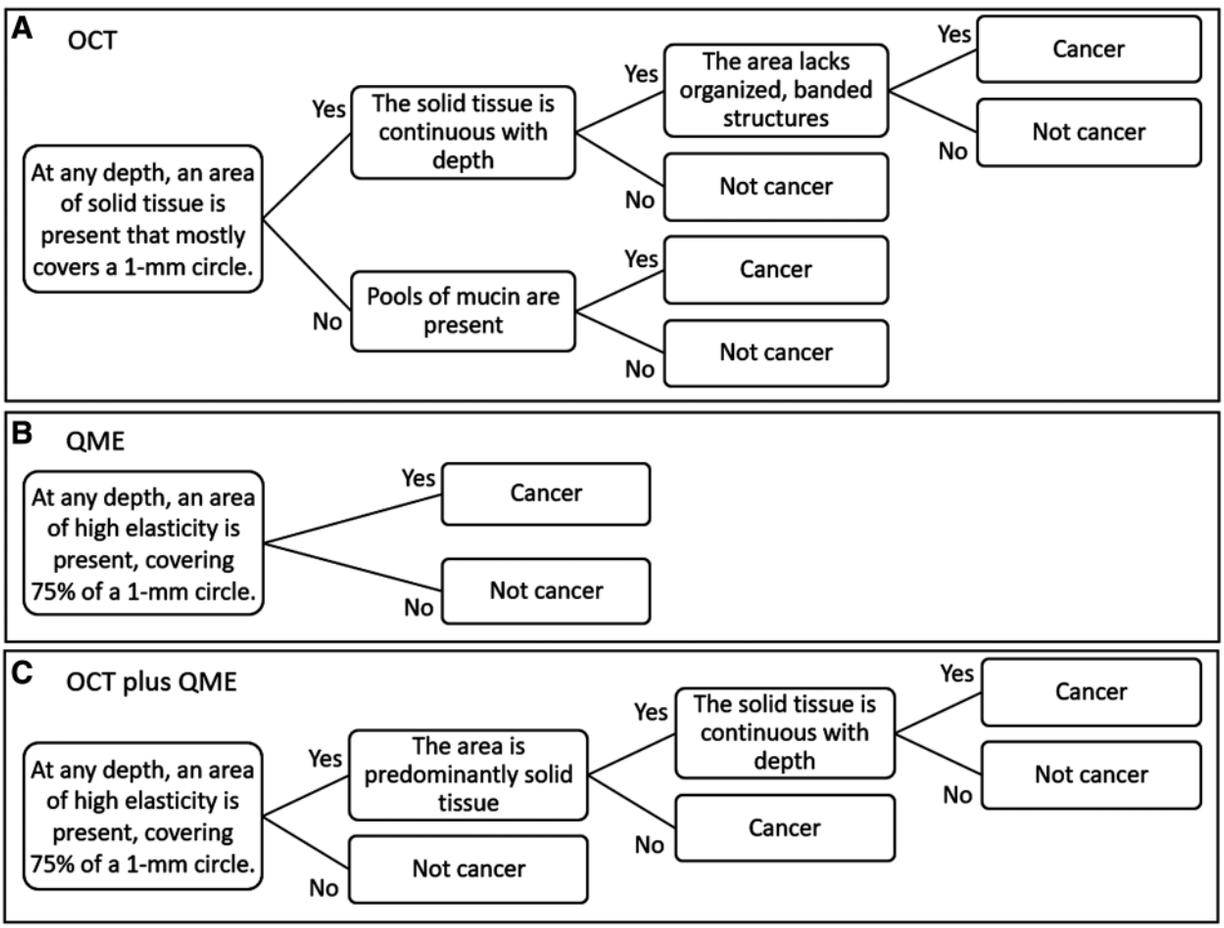

Figure 1.
Reader criteria for determining presence of cancer. Criteria for cancer using OCT images (**A**), QME images (**B**), OCT and QME combined (**C**).

mucinous carcinoma (present in four recruited patients), in which tumor cells produce pools of a liquid substance known as mucin. Mucinous pools result in regions of low signal in OCT images, appearing similar to adipose tissue, but can often be identified by the outline of the pool, which has higher OCT signal. Thus, readers evaluated OCT images for the presence of these structures, even if at first it appeared that the tissue was adipose tissue (bottom path, **Fig 1A**).

In QME images, readers were trained to look for areas of high elasticity, based on studies across spatial scales showing that cancer and its associated stroma are stiffer than benign tissues (36, 37, 44). To avoid mistaking small, isolated patches of stiff stroma for cancer, the region of high elasticity had to cover at least 75% of a 1-mm diameter circle (**Fig. 1B**). This diameter was chosen empirically based on analysis of how tumor presented in QME images both in previous studies (43, 44) and in the training data. The user interface enabled readers to calculate this precisely by dragging their cursor to any location in the ROI. High elasticity was defined as >26.3 kPa, based on analysis of prior and current study data and is denoted by a black line on the color scale of all presented QME images. To assess OCT + QME in combination, readers were again directed to assess continuity with depth and ensure that the region was solid tissue, in addition to the elasticity criterion (**Fig. 1C**). Mucinous carcinoma presented a special scenario (second step in **Fig. 1C**): if an area had high elasticity but appeared in the OCT to lack "solid tissue," this was likely a mucinous carcinoma, and, as such, results in "cancer" in the decision tree. This was based on our observation that even these liquid-dominant tumors resulted in high elasticity, likely due to interstitial fluid pressure within the tissue.

Finally, the QME criterion, facilitated by its quantitative nature, was implemented into a preliminary automated algorithm. This involved thresholding the elasticity values in the QME images at every depth to generate binary images (with ones representing pixels with an elasticity >26.3 kPa), then convolving these binary images with a 1 mm diameter circular kernel. The values at each pixel in the kernel were normalized such that the result of the convolution equaled the percentage of the circle covered by high elasticity. If, for a given ROI, the convolution produced a value ≥75% at any location in the ROI, that ROI was interpreted as containing cancer. As such, this algorithm was equivalent to the QME reader criteria shown in **Fig. 1B**. This algorithm was implemented on a standard desktop computer using MATLAB (Mathworks, R2016a), and took approximately one minute to read all ROIs.

Following the readings, the sensitivity, specificity, positive predictive value (PPV), negative predictive value (NPV), and accuracy were calculated for each reader. 95% confidence intervals were estimated using the score interval for a binomial case ("Wald" interval; ref. 49). Aggregates were computed by taking the sum of the individual results of the seven readers (the totals of true positive, false positive, true negative, and false negative counts), and computing the sensitivity, specificity, PPV, NPV, accuracy, and confidence intervals on these summed totals. The performance of QME and OCT plus QME were compared against OCT alone using McNemar test (50) for statistical significance. Interreader agreement was quantified using the Fleiss' Kappa metric (51). Detailed statistical calculations are provided in Supplementary Reader Statistics.

Results

OCT and QME images of malignant and benign breast tissues at the margin

Intact BCS specimens from 71 patients were scanned for the reader study, without any damage to the tissue nor disruption to typical histopathologic protocol. One hundred and seventy-four ROIs from the 71 patients were selected and coregistered with histology. Of these, 154 ROIs were included in the reader study. **Table 2** summarizes the tissue types and characteristics of the included ROIs. Reasons for exclusion were extensive thermal damage, as determined by postoperative histology ($n = 3$); inconclusive registration with histology sections ($n = 4$); insufficient contact between the specimen, silicone layer, and the imaging window ($n = 3$); imaging artifacts (*e.g.*, stray reflections or surgical clips precluded image interpretation, $n = 4$); insufficient elasticity data overlaid on solid tissue ($n = 2$); a rare form of mucinous DCIS (insufficient data to build decision criteria, $n = 2$); and the region of tumor within the ROI having a size <1 mm ($n = 2$). Of the 154 ROIs included in this study, 24 had cancer within 1 mm of the surface, corresponding to a prevalence of 15.6%. Most were made up of a mix of tissue types, including adipose tissue, stroma, and parenchymal tissues. See Supplementary Table S2 and "Note on prevalence" in Supplementary Information for more details on tumor prevalence.

Table 2. Summary of regions of interest included in study.

ROI selection	Number	
Imaged margins	139	
ROIs coregistered with histology	174	
ROIs included in reader study	154	
Tissue types in included ROIs		**Percentage (/154)**
Cancer within 1 mm (positive ROI)	**24**	**15.6%**
Invasive (solid)	14	9.1%
Invasive (mucinous)	3	1.9%
DCIS	7	4.5%
Clear within 1 mm (negative ROI)	**130**	**84.4%**
Predominantly adipose tissue	38	24.7%
Adipose tissue with dense stroma	37	24.0%
Adipose tissue with ducts/vessels	24	15.6%
Adipose tissue with strands of connective tissue	19	12.3%
Dense stroma	12	7.8%

Figures 2 to 4 present ROIs from the reader study, representative of the various tissue types encountered in the study. In each case, *en face*, 10 × 10 mm OCT and QME images are displayed at a depth of 40 to 60 μm (entire 3D volumes available in Supplementary Videos S1–S6), along with the corresponding hematoxylin and eosin histology. The plane and orientation of the histology is indicated by the red dashed line in each set of images.

Figure 2 shows ROIs containing benign breast tissues: adipose tissue (**Fig. 2A–C**) and a mix of adipose tissue and stroma containing benign ducts (**Fig. 2D–F**). The OCT in **Fig. 2A** (Supplementary Video S1) depicts the honeycomb structure typical of adipose tissue. Thin strands of connective tissue are present throughout this ROI, and QME shows that the elasticity in these regions tends to be low (**Fig. 2B**). Six of seven readers called this benign using OCT alone, compared to all readers using QME combined with OCT. A larger region of benign stroma is shown at the margin in **Fig. 2D**, and 3D analysis reveals that this structure lacks continuity, with intermittent adipose tissue present with depth (Supplementary Video S2), similar to the pattern in the histology image (**Fig. 2F**). However, using OCT alone, three readers incorrectly assessed this as cancer. In QME (**Fig. 2E**), this stroma exhibits mostly low elasticity. Very small pockets of high elasticity are seen at a few points throughout the stroma, but only features with more widespread elasticity were

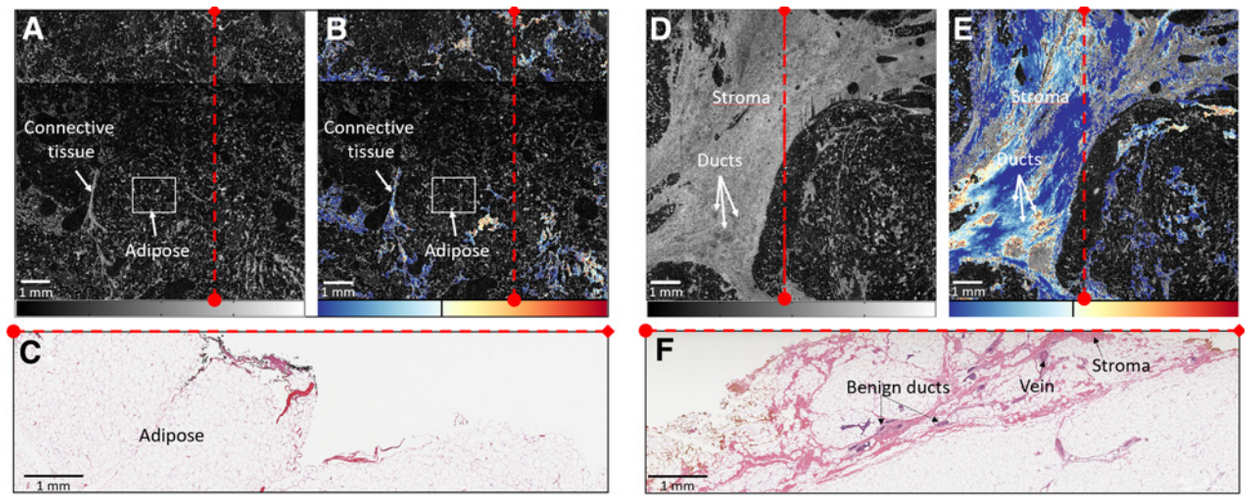

Figure 2.

Example images of benign breast tissues. OCT (**A**), QME (**B**), and hematoxylin and eosin histology (**C**) of adipose tissue with thin strands of stroma; OCT (**D**), QME (**E**), and hematoxylin and eosin histology (**F**) of a large region of benign stroma and adipose tissue. Color bars, OCT 0–40 dB; Elasticity 3.63–363 kPa.

considered suspicious for cancer. All seven readers correctly called this benign using QME and QME plus OCT.

Figure 3 shows positive ROIs from two BCS cases, each containing invasive ductal carcinoma on the margin. In **Fig. 3C**, the histology image reveals invasive ductal carcinoma grade 3 with high cellular density, surrounded by adipose tissue. Correspondingly, the OCT (**Fig. 3A**) captured a region of solid tissue with a nodular appearance (no indication of striated, organized collagen) that matches the location of tumor in the histology image. In QME (**Fig. 3B**), this region shows elevated elasticity, due to the much higher cellular density in the tumor compared with the surrounding adipose tissue. This detected region of tumor is approximately 2 mm across, making up <0.2% of the total surface area of this particular margin, demonstrating the high resolution of the technique. All seven readers evaluated this ROI correctly using OCT, QME, and the combination. The histology image in **Fig. 3F** shows invasive ductal carcinoma grade III surrounded by a mix of stroma and adipose tissue. A mix of adipose tissue and solid tissue is also present in the OCT image (**Fig. 3D**), and QME reveals a portion of the solid tissue to have high elasticity (**Fig. 3E**). 3D analysis of the images (Supplementary Video 4) shows that the region with high elasticity is also continuous with depth (i.e., adipose tissue is not revealed underneath). On the basis of OCT alone, one of the seven readers called this as a false negative, mistaking it for benign, whereas all seven readers evaluated this as cancer using QME alone or alongside OCT.

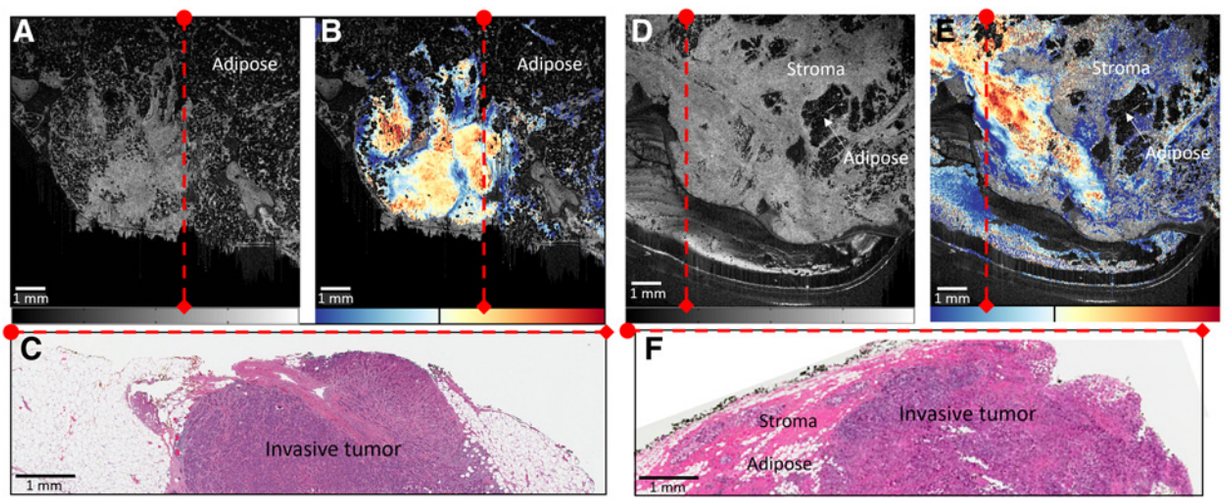

Figure 3.

Example images of invasive ductal carcinoma. OCT (**A**), QME (**B**), and hematoxylin and eosin histology (**C**) of highly cellular invasive ductal carcinoma on the margin; OCT (**D**), QME (**E**), and hematoxylin and eosin histology (**F**) of invasive ductal carcinoma on the margin surrounded by adipose tissue and stromal tissues. Color bars, OCT 0–40 dB; elasticity 3.63–363 kPa.

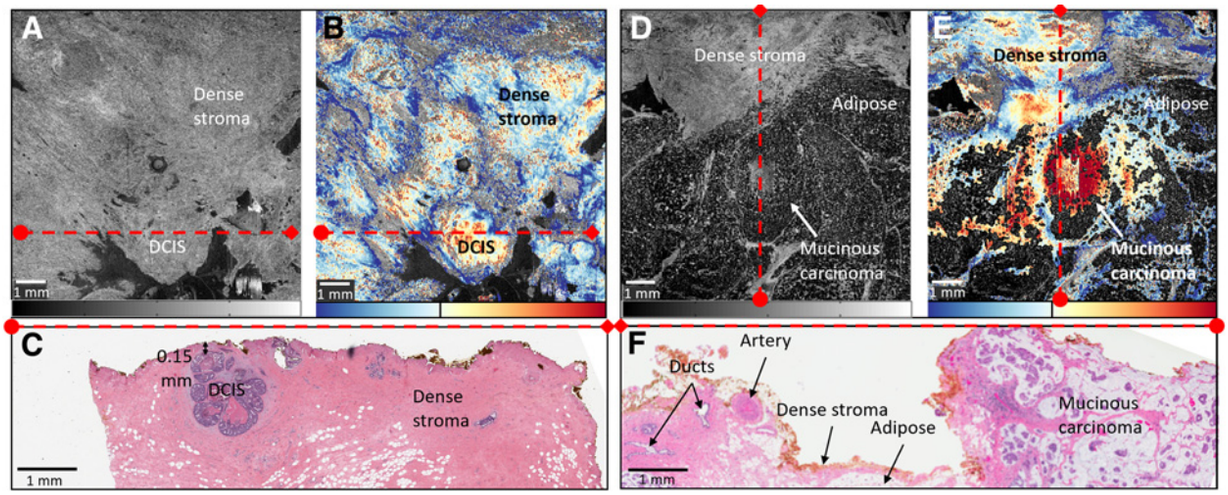

Figure 4.

Example images of DCIS and mucinous carcinoma. OCT (**A**), QME (**B**), and hematoxylin and eosin histology (**C**) of DCIS 0.15 mm from the margin; OCT (**D**), QME (**E**), and hematoxylin and eosin histology (**F**) of invasive mucinous carcinoma present on the margin. Color bars, OCT 0–40 dB; elasticity 3.63–363 kPa.

Figure 4 shows ROIs containing two malignant tissue types: DCIS (**Fig. 4A–C**) and mucinous carcinoma (**Fig. 4D–F**), which were designated "impalpable" preoperatively and required hookwire guidance for lesion excision. Despite being impalpable on a macroscale, changes in mechanical properties on a microscale are detectable by QME for these tissue types (43). **Figure 4A–C** shows an example of DCIS within 0.15 mm of the margin; the histology image (**Fig. 4C**) shows the involved duct surrounded by dense, benign stroma. The OCT (**Fig. 4A**) shows no apparent contrast between this duct and the surrounding stroma, but the QME (**Fig. 4B**) highlights high elasticity corresponding to the region of DCIS. This elevated elasticity corresponds to the dense, proliferating cells within the duct, as well as a fibrotic stromal response (52) immediately surrounding the duct. Throughout the stroma in the rest of the ROI, there are small, localized areas of elevated elasticity, but most do not meet the size criterion for cancer defined in this study. Six of seven readers evaluated this correctly using OCT alone, as the structure shows continuity with depth (Supplementary Video S5), and all readers evaluated it correctly using QME. In **Fig. 4D–F** (Supplementary Video S6), a region of benign stroma and adipose tissue neighbors a region of mucinous carcinoma on the margin. In OCT (**Fig. 4D**), the region corresponding to the mucinous tumor is difficult to distinguish from the surrounding adipose tissue, and one reader designated this as benign. However, in QME (**Fig. 4E**) the tumor exhibits elevated elasticity, and all readers correctly classified this ROI as cancerous when QME was available.

Blinded reader study results in higher accuracy using QME over OCT alone

Table 3 and Supplementary Fig. S3 summarize the results of the reader study. Readers completed evaluation of the 154 OCT plus QME ROIs in an average of 4 hours, or approximately 90 seconds per ROI. Interreader agreement was nearly perfect for QME and OCT plus QME, and moderate for OCT alone, according to a standard interpretation of the Fleiss' Kappa index for interrater agreement. Reported ranges for sensitivity and specificity in **Table 3** indicate 95% confidence intervals. On the basis of the aggregate results, the sensitivity, specificity, and accuracy of OCT for detecting cancer within 1 mm of the margin were 69.0%, 79.0%, and 77.5%, respectively. Using QME, sensitivity, specificity, and accuracy were 92.9%, 96.4%, and 95.8%, respectively. Using combined OCT and QME criteria, sensitivity, specificity, and accuracy were 80.4%, 99.5%, and 96.5%, respectively. Sensitivity was significantly ($P < 0.05$) improved using QME over OCT alone for 6 of the 7 readers, and specificity was significantly improved using QME over OCT alone for all 7 readers (see Supplementary Reader Statistics for calculations).

Also reported in **Table 3**, the automated reader for QME resulted in 100.0%, 97.7%, and 98.1% sensitivity, specificity, and accuracy, respectively.

Discussion

This study is the first to determine the accuracy of QME, or any variant of optical elastography, for assessment of tumor margins in specimens excised during BCS. Prior to this study, recent investigations had demonstrated that QME has the potential to delineate tumor in breast tissue based on elevated elasticity on a microscale (43, 44). In these studies, as in this one, the contrast between tumor and healthy tissue based on changes in elasticity was shown to be complementary to the structural contrast provided by the underlying modality, OCT. However, prior studies had not investigated the ability of QME to identify positive margins in specimens from BCS. This study has demonstrated high accuracy of QME (96%) compared with OCT (78%) for detecting cancer within 1 mm of the margin in BCS specimens. The measurements here, on intact BCS specimens immediately following surgery, are also of high clinical relevance, compared with prior OCT studies that relied primarily on dissected mastectomy specimens for testing novel margin assessment techniques (27, 28, 46).

The QME results here indicate that tissue elasticity is an accurate predictor of malignancy. This trend was consistent across multiple tumor types in this study (e.g., solid and mucinous invasive carcinomas, and DCIS), although this must be confirmed with larger sample sizes of each tumor type. Future data collection will also continue to elucidate the sources of elevated elasticity in

Table 3. Reader study results.

	OCT					QME					OCT + QME				
Reader	**Sensitivity**	**Specificity**	**PPV**	**NPV**	**Acc**	**Sensitivity**	**Specificity**	**PPV**	**NPV**	**Acc**	**Sensitivity**	**Specificity**	**PPV**	**NPV**	**Acc**
Eng 1	62.5 ± 19.4%	85.4 ± 6.1%	44%	93%	82%	100.0 ± 0.0%	97.7 ± 2.6%	89%	100%	98%	87.5 ± 13.2%	100 ± 0.0%	100%	98%	98%
Eng 2	70.8 ± 18.2%	86.9 ± 5.8%	50%	94%	84%	100.0 ± 0.0%	97.7 ± 2.6%	89%	100%	98%	87.5 ± 13.2%	100 ± 0.0%	100%	98%	98%
Surg 1	62.5 ± 19.4%	74.6 ± 7.5%	31%	92%	73%	75.0 ± 17.3%	88.5 ± 5.5%	55%	95%	86%	70.8 ± 18.2%	96.9 ± 3.0%	81%	95%	93%
Surg 2	66.7 ± 18.9%	72.3 ± 7.7%	31%	92%	71%	95.8 ± 8.0%	97.7 ± 2.6%	89%	99%	97%	95.8 ± 8.0%	100 ± 0.0%	100%	99%	99%
Path	66.7 ± 18.9%	83.8 ± 6.3%	43%	93%	81%	95.8 ± 8.0%	97.7 ± 2.6%	89%	99%	97%	70.8 ± 18.2%	100 ± 0.0%	100%	95%	96%
Res	79.2 ± 16.2%	74.6 ± 7.5%	37%	95%	75%	87.5 ± 13.2%	97.7 ± 2.6%	88%	98%	96%	66.7 ± 18.9%	99.2 ± 1.5%	94%	94%	94%
Sonog	75.0 ± 17.3%	75.4 ± 7.4%	36%	94%	75%	95.8 ± 8.0%	97.7 ± 2.6%	89%	99%	97%	83.3 ± 14.9%	100 ± 0.0%	100%	97%	97%
Agg	69.0 ± 7.0%	79.0 ± 2.6%	38%	93%	78%	92.9 ± 3.9%	96.4 ± 1.2%	83%	99%	96%	80.4 ± 6.0%	99.5 ± 0.5%	96%	97%	97%
Automated reader						100.0 ± 0.0%	97.7 ± 2.6%	89%	100%	98%					

Abbreviations: Acc, accuracy; Agg, aggregate; Eng, engineer; Surg, surgeon; Path, pathology scientist; Res, medical resident; Sonog, sonographer.

each tumor type, for example, deposition of stiff desmoplastic stroma, changes in collagen alignment, or interstitial fluid pressure. Better understanding of these mechanisms may foster even greater precision in the use of QME to detect various tumor types intraoperatively. This goal may be facilitated by implementing ultrahigh resolution QME to achieve cellular-scale elasticity resolution (53, 54).

Perhaps counterintuitively, although combining OCT and QME improved overall accuracy compared with OCT alone, the sensitivity using the high elasticity criterion (93%) was greater than that using QME and OCT criteria together (80%). This may be due to variability in reader interpretation of the qualitative OCT criteria (interpretation of structures) versus little variability in interpretation of the quantitative QME criterion (elasticity threshold). In particular, analysis of reader notes revealed variability in whether readers considered features as "continuous" with depth based on OCT (**Fig. 1A**), which was requisite in this study for an ROI to be considered positive (the engineers who participated as readers had prior experience in reading OCT and elastography images, which may have contributed to their slightly superior reading performance). On the other hand, specificity of OCT and QME together (∼100%) was greater than that of QME (96%) or OCT (79%) alone, indicating that the combination of information reduces false positives (e.g., mistaking benign, fibrous stroma for cancer). To improve intraoperative margin assessment and ultimately reduce the need for costly repeat surgeries, high sensitivity is essential to ensuring that less cancer is missed (i.e., minimizing false negatives). High specificity, on the other hand, ensures that less benign tissue is unnecessarily removed, and, while important to avoid overtreatment of the cancer, could be considered secondary to the need for high sensitivity in margin assessment. QME showed the best overall performance on both sides, but future studies will need to analyze the amount of repeat surgeries avoided versus extra volumes of tissue removed.

Although the accuracy of OCT reported here is similar to that reported in another study in BCS specimens (30), further refinement and quantification of OCT criteria may potentially increase accuracy in future studies. For instance, quantification of the rate of OCT signal attenuation with depth has shown potential for distinguishing benign and malignant regions (28, 32), although it is not clear the extent to which this will improve accuracy. Our preliminary automation of QME reading could also be extended to incorporate both QME and OCT-based information into an algorithm utilizing neural networks.

Although the spatial resolution of OCT and QME images is on the order of micrometers (Supplementary Fig. S4), which is comparable or superior to many existing intraoperative margin assessment techniques, readers were directed to ignore features smaller than approximately 1 mm. This set an effective "diagnostic resolution" of approximately 1 mm, and further study is needed to assess the accuracy of OCT and QME for smaller features, such as very early stage DCIS. However, at a more advanced stage, DCIS tends to result in dilation of ducts, and even small ducts can result in a fibrous stromal response in the surrounding tissue (52); thus, QME is expected to be sensitive to the associated mechanical changes caused by these features. The resolution of the technique may also improve in the future using the inverse method to solve for elasticity (55, 56), rather than rely on assumptions of stress uniformity with depth, as in our current method; however, computation times currently prohibit this from being implemented in clinically feasible timeframes.

Although the results presented here demonstrate the potential of QME for margin assessment in BCS, additional development is required to address the exclusion criteria described in the Results section. In particular, ROIs were excluded because of thermal damage, insufficient contact between the specimen, silicone layer and the imaging window, imaging artifacts and insufficient elasticity data overlaid on solid tissue. In the case of thermal damage, future studies could mitigate its presence in the images by using combined contrast from QME and OCT, including investigation of textural analysis, as well as colorimetric data from photographs simultaneously taken of the specimen (Supplementary Fig. S1), which often show black marks on the tissue surface that may correspond to thermal damage.

Two margins per specimen were imaged in this study, at a rate of approximately 9 minutes per margin. In some specimens, postoperative histology revealed cancer within 1 mm on margins that were not scanned, leading to a discrepancy in the overall prevalence of close margins reported in **Table 1** (45%) and the prevalence of ROIs containing cancer (15.6%). Additional details on prevalence are provided in Supplementary Table S2. To facilitate rapid intrao-

perative QME of all radial margins, which is desirable in the clinical scenario, higher acquisition speed has been achieved using a novel approach (57), and may be further increased by implementation of high-speed OCT systems, an order of magnitude faster than that in this study (58). In addition, reader evaluation of the images took 90 seconds on average, which is conducive to clinical timeframes. However, to enable entire margins to be analyzed intraoperatively will require the development of image processing algorithms that facilitate more rapid image interpretation. Finally, a handheld probe is in development to allow QME assessment of tissues directly within the surgical cavity and to facilitate implementation into the clinical workflow (59).

In this study, analogously to previous studies (27, 30), we selected ROIs ($n = 154$) on which the reader study was performed rather than performing the study on entire margins. Of utmost importance to our reader study is the ability to correspond reader ratings to a ground truth. Without ground truth histology correspondence to our images, we have no basis to classify regions as tumor or nontumor. As the histology protocol used at our hospital enabled histology matching on only a small subset of each margin, the ROI approach was required. As this study has demonstrated strong correspondence between high elasticity and corresponding co-registered tumor, a next step is to perform a reader study on entire margins.

In summary, QME, an emerging OCT elastography technique that probes tissue elasticity on the microscale, has demonstrated detection of close and positive margins in freshly excised specimens in BCS with 93% sensitivity and 96% specificity. The use of intrinsic tissue contrast without need for exogenous dyes and the optimal trade-off in speed, field of view, and resolution provided by QME make it a promising candidate for improving intraoperative guidance of BCS. More broadly, QME may be applicable in a range of surgical or preoperative biopsy guidance applications, particularly in cancers that are known to exhibit altered mechanical properties.

Disclosure of Potential Conflicts of Interest

K.M. Kennedy is a consultant at OncoRes Medical. L. Chin has ownership interest (including patents) in OncoRes Medical. A. Curatolo is a consultant at OncoRes Medical Pty and has ownership interest (including patents) in OncoRes Medical Pty. S.L. Chin is an advisor at OncoRes Medical. K. Giles is the CEO at OncoRes Medical and has ownership interest (including patents) in OncoRes Medical. B. Latham has ownership interest (including patents) in OncoRes. B.F. Kennedy is the chief scientific officer at, reports receiving a commercial research grant from, and has ownership interest (including patents) in OncoRes Medical. No potential conflicts of interest were disclosed by the other authors.

Authors' Contributions

Conception and design: K.M. Kennedy, W.M. Allen, B. Latham, C.M. Saunders, B.F. Kennedy

Development of methodology: K.M. Kennedy, R. Zilkens, W.M. Allen, L. Chin, H. DeJong, C.M. Saunders, B.F. Kennedy

Acquisition of data (provided animals, acquired and managed patients, provided facilities, etc.): K.M. Kennedy, R. Zilkens, W.M. Allen, Q. Fang, L. Chin, R.W. Sanderson, H.E.I. Tan, B. Kunjuraman, C. Yeomans, S.L. Chin, H. DeJong, B.F. Dessauvagie, B. Latham, C.M. Saunders, B.F. Kennedy

Analysis and interpretation of data (e.g., statistical analysis, biostatistics, computational analysis): K.M. Kennedy, R. Zilkens, W.M. Allen, K.Y. Foo, L. Chin, P. Wijesinghe, A. Curatolo, N. Morin, C. Yeomans, S.L. Chin, K. Giles, B.F. Dessauvagie, B. Latham, C.M. Saunders, B.F. Kennedy

Writing, review, and/or revision of the manuscript: K.M. Kennedy, R. Zilkens, W.M. Allen, K.Y. Foo, Q. Fang, L. Chin, J. Anstie, P. Wijesinghe, A. Curatolo, H.E.I. Tan, B. Kunjuraman, S.L. Chin, H. DeJong, K. Giles, B.F. Dessauvagie, B. Latham, C.M. Saunders, B.F. Kennedy

Administrative, technical, or material support (i.e., reporting or organizing data, constructing databases): R. Zilkens, W.M. Allen, L. Chin, H.E.I. Tan, C. Yeomans

Study supervision: C.M. Saunders, B.F. Kennedy

Acknowledgments

We gratefully acknowledge Dr. Max Bulsara from University of Notre Dame Australia for discussion of biostatistics. We acknowledge funding from OncoRes Medical and the Department of Health Western Australia.

The costs of publication of this article were defrayed in part by the payment of page charges. This article must therefore be hereby marked *advertisement* in accordance with 18 U.S.C. Section 1734 solely to indicate this fact.

Received April 20, 2019; revised August 9, 2019; accepted February 14, 2020; published first April 15, 2020.

References

1. Landercasper J, Attai D, Atisha D, Beitsch P, Bosserman L, Boughey J, et al. Toolbox to reduce lumpectomy reoperations and improve cosmetic outcome in breast cancer patients: the American society of breast surgeons consensus conference. Ann Surg Oncol 2015;22:3174–83.
2. Landercasper J, Whitacre E, Degnim AC, Al-Hamadani M. Reasons for re-excision after lumpectomy for breast cancer: insight from the American Society of Breast Surgeons Mastery SM database. Ann Surg Oncol 2014;21:3185–91.
3. McCahill LE, Single RM, Bowles EJA, Feigelson HS, James TA, Barney T, et al. Variability in reexcision following breast conservation surgery. JAMA 2012;307:467–75.
4. Kimball CC, Nichols CI, Vose JG. The payer and patient cost burden of open breast conserving procedures following percutaneous breast biopsy. Breast Cancer (Auckl) 2018;12:1178223418777766.
5. Metcalfe LN, Zysk AM, Yemul KS, Jacobs LK, Oker EE, Underwood HR, et al. Beyond the margins—economic costs and complications associated with repeated breast-conserving surgeries. JAMA Surg 2017;152:1084–6.
6. Esbona K, Li Z, Wilke LG. Intraoperative imprint cytology and frozen section pathology for margin assessment in breast conservation surgery: a systematic review. Ann Surg Oncol 2012;19:3236–45.
7. Decker MR, Trentham-Dietz A, Loconte NK, Neuman HB, Smith MA, Punglia RS, et al. The role of intraoperative pathologic assessment in the surgical management of ductal carcinoma in situ. Ann Surg Oncol 2016;23:2788–94.
8. Harness JK, Giuliano AE, Pockaj BA, Downs-Kelly E. Margins: a status report from the Annual Meeting of the American Society of Breast Surgeons. Ann Surg Oncol 2014;21:3192–7.
9. Miller CL, Coopey SB, Rafferty E, Gadd M, Smith BL, Specht MC. Comparison of intra-operative specimen mammography to standard specimen mammography for excision of non-palpable breast lesions: a randomized trial. Breast Cancer Res Treat 2016;155:513–9.
10. Rhee D, Pockaj B, Wasif N, Stucky C-C, Pizzitola V, Giurescu M, et al. Operative outcomes of conventional specimen radiography versus in-operating room specimen radiography in radioactive seed-localized segmental mastectomies. Am J Surg 2018;215:151–4.
11. Britton P, Sonoda L, Yamamoto A, Koo B, Soh E, Goud A. Breast surgical specimen radiographs: how reliable are they? Eur J Radiol 2011;79:245–9.
12. Layfield DM, May DJ, Cutress RI, Richardson C, Agrawal A, Wise M, et al. The effect of introducing an in-theatre intra-operative specimen radiography (IOSR)

system on the management of palpable breast cancer within a single unit. Breast 2012;21:459–63.
13. Krekel NM, Haloua MH, Cardozo AML, de Wit RH, Bosch AM, de Widt-Levert LM, et al. Intraoperative ultrasound guidance for palpable breast cancer excision (COBALT trial): a multicentre, randomised controlled trial. Lancet Oncol 2013; 14:48–54.
14. Ramos M, Díaz JC, Ramos T, Ruano R, Aparicio M, Sancho M, et al. Ultrasound-guided excision combined with intraoperative assessment of gross macroscopic margins decreases the rate of reoperations for non-palpable invasive breast cancer. Breast 2013;22:520–4.
15. Ahmed M, Douek M. Intra-operative ultrasound versus wire-guided localization in the surgical management of non-palpable breast cancers: systematic review and meta-analysis. Breast Cancer Res Treat 2013;140: 435–46.
16. Olsha O, Shemesh D, Carmon M, Sibirsky O, Dalo RA, Rivkin L, et al. Resection margins in ultrasound-guided breast-conserving surgery. Ann Surg Oncol 2011; 18:447–52.
17. Pappo I, Spector R, Schindel A, Morgenstern S, Sandbank J, Leider LT, et al. Diagnostic performance of a novel device for real-time margin assessment in lumpectomy specimens. J Surg Res 2010;160:277–81.
18. Schnabel F, Boolbol SK, Gittleman M, Karni T, Tafra L, Feldman S, et al. A randomized prospective study of lumpectomy margin assessment with use of MarginProbe in patients with nonpalpable breast malignancies. Ann Surg Oncol 2014;21:1589–95.
19. Lamberts LE, Koch M, de Jong JS, Adams AL, Glatz J, Kranendonk ME, et al. Tumor-specific uptake of fluorescent bevacizumab–IRDye800CW microdosing in patients with primary breast cancer: a phase1 feasibility study. J Clin Cancer Res 2017;23:2730–41.
20. Tummers QR, Verbeek FP, Schaafsma BE, Boonstra MC, van der Vorst JR, Liefers G-J, et al. Real-time intraoperative detection of breast cancer using near-infrared fluorescence imaging and methylene blue. Eur J Surg Oncol 2014;40: 850–8.
21. Unkart JT, Chen SL, Wapnir IL, González JE, Harootunian A, Wallace AM. Intraoperative tumor detection using a ratiometric activatable fluorescent peptide: a first-in-human phase 1 study. Ann Surg Oncol 2017;24: 3167–73.
22. Whitley MJ, Cardona DM, Lazarides AL, Spasojevic I, Ferrer JM, Cahill J, et al. A mouse-human phase 1 co-clinical trial of a protease-activated fluorescent probe for imaging cancer. Sci Transl Med 2016;8: 320ra4–ra4.
23. Wang YW, Reder NP, Kang S, Glaser AK, Yang Q, Wall MA, et al. Raman-encoded molecular imaging with topically applied SERS nanoparticles for intraoperative guidance of lumpectomy. Cancer Res 2017;77:4506–16.
24. Brown JQ, Bydlon TM, Kennedy SA, Caldwell ML, Gallagher JE, Junker M, et al. Optical spectral surveillance of breast tissue landscapes for detection of residual disease in breast tumor margins. PLoS One 2013;8:e69906.
25. Kho E, de Boer LL, Van de Vijver K, van Duijnhoven F, Vrancken Peeters M-JTFD, Sterenborg HJCM, et al. Hyperspectral imaging for resection margin assessment during cancer surgery. Clin Cancer Res 2019;25:3572–80.
26. Shipp DW, Rakha EA, Koloydenko AA, Macmillan RD, Ellis IO, Notingher I. Intra-operative spectroscopic assessment of surgical margins during breast conserving surgery. Breast Cancer Res 2018;20:69.
27. Erickson-Bhatt SJ, Nolan RM, Shemonski ND, Adie SG, Putney J, Darga D, et al. Real-time imaging of the resection bed using a handheld probe to reduce incidence of microscopic positive margins in cancer surgery. Cancer Res 2015;75:3706.
28. Ha R, Friedlander LC, Hibshoosh H, Hendon C, Feldman S, Ahn S, et al. Optical coherence tomography: A novel imaging method for post-lumpectomy breast margin assessment—A multi-reader study. Acad Radiol 2018;25:279–87.
29. Yao X, Gan Y, Chang E, Hibshoosh H, Feldman S, Hendon C. Visualization and tissue classification of human breast cancer images using ultrahigh resolution OCT. Lasers Surg Med 2017;49:258–69.
30. Zysk AM, Chen K, Gabrielson E, Tafra L, May Gonzalez EA, Canner JK, et al. Intraoperative assessment of final margins with a handheld optical imaging probe during breast-conserving surgery may reduce the reoperation rate: results of a multicenter study. Ann Surg Oncol 2015;22: 3356–62.
31. Kennedy BF, McLaughlin RA, Kennedy KM, Chin L, Wijesinghe P, Curatolo A, et al. Investigation of optical coherence micro-elastography as a method to visualize cancers in human breast tissue. Cancer Res 2015; 75:3236–3245.
32. Scolaro L, McLaughlin RA, Kennedy BF, Saunders CM, Sampson DD. A review of optical coherence tomography in breast cancer. Photonics Lasers Med 2014;3: 225–40.
33. Zhou C, Cohen DW, Wang Y, Lee HC, Mondelblatt AE, Tsai TH, et al. Integrated optical coherence tomography and microscopy for ex vivo multiscale evaluation of human breast tissues. Cancer Res 2010;70:10071.
34. Maloney BW, McClatchy DM, Pogue BW, Paulsen KD, Wells WA, Barth RJ. Review of methods for intraoperative margin detection for breast conserving surgery. J Biomed Opt 2018;23:1–19.
35. McEvoy MP, Landercasper J, Naik HR, Feldman S. Update of the American society of breast surgeons toolbox to address the lumpectomy reoperation epidemic. Gland Surg 2018;7:536.
36. Krouskop TA, Wheeler TM, Kallel F, Garra BS, Hall T. Elastic moduli of breast and prostate tissues under compression. Ultrason Imaging 1998;20: 260–74.
37. Plodinec M, Loparic M, Monnier CA, Obermann EC, Zanetti-Dallenbach R, Oertle P, et al. The nanomechanical signature of breast cancer. Nat Nanotechnol 2012;7:757–65.
38. Wojcinski S, Farrokh A, Weber S, Thomas A, Fischer T, Slowinski T, et al. Multicenter study of ultrasound real-time tissue elastography in 779 cases for the assessment of breast lesions: improved diagnostic performance by combining the BI-RADS¬Æ-US classification system with sonoelastography. Ultraschall Med 2010;31:484–91.
39. Dua SM, Gray RJ, Keshtgar M. Strategies for localisation of impalpable breast lesions. Breast 2011;20:246–53.
40. Xu H, Varghese T, Jiang J, Zagzebski JA. In vivo classification of breast masses using features derived from axial-strain and axial-shear images. Ultrason Imaging 2012;4:222–36.
41. Kennedy BF, Wijesinghe P, Sampson DD. The emergence of optical elastography in biomedicine. Nat Photonics 2017;11:215.
42. Allen WM, Foo KY, Zilkens R, Kennedy KM, Fang Q, Chin L, et al. Clinical feasibility of optical coherence micro-elastography for imaging tumor margins in breast-conserving surgery. Biomed Opt Express 2018;9: 6331–49.
43. Kennedy KM, Chin L, McLaughlin RA, Latham B, Saunders CM, Sampson DD, et al. Quantitative micro-elastography: imaging tissue elasticity using compression optical coherence elastography. Sci Rep 2015;5:15538.
44. Allen WM, Kennedy KM, Fang Q, Chin L, Curatolo A, Watts L, et al. Wide-field quantitative micro-elastography of human breast tissue. Biomed Opt Express 2018;9:1082–96.
45. Schneider CA, Rasband WS, Eliceiri KW. NIH Image to ImageJ: 25 years of image analysis. Nat Methods 2012;9:671.
46. Assayag O, Antoine M, Sigal-Zafrani B, Riben M, Harms F, Burcheri A, et al. Large field, high resolution full-field optical coherence tomography: a pre-clinical study of human breast tissue and cancer assessment. Technol Cancer Res Treat 2014;13:455–68.
47. Nguyen FT, Zysk AM, Chaney EJ, Kotynek JG, Oliphant UJ, Bellafiore FJ, et al. Intraoperative evaluation of breast tumor margins with optical coherence tomography. Cancer Res 2009;69:8790.
48. Yemul KS, Zysk AM, Richardson AL, Tangella KV, Jacobs LK. Interpretation of optical coherence tomography images for breast tissue assessment. Surg Innov 2019;26:50–6.
49. Brown LD, Cai TT, DasGupta A. Interval estimation for a binomial proportion. Statist Sci 2001;16:101–17.
50. Kim S, Lee W. Does McNemar's test compare the sensitivities and specificities of two diagnostic tests? Stat Methods Med Res 2017;26: 142–54.
51. Fleiss JL. Measuring nominal scale agreement among many raters. Psychol Bull 1971;76:378.
52. Sharma M, Beck AH, Webster JA, Espinosa I, Montgomery K, Varma S, et al. Analysis of stromal signatures in the tumor microenvironment of ductal carcinoma *in situ*. Breast Cancer Res Treat 2010;123:397–404.
53. Curatolo A, Villiger M, Lorenser D, Wijesinghe P, Fritz A, Kennedy BF, et al. Ultrahigh resolution optical coherence elastography. Opt Lett 2016; 41:21–4.
54. Wijesinghe P, Johansen NJ, Curatolo A, Sampson DD, Ganss R, Kennedy BF. Ultrahigh-resolution optical coherence elastography images cellular-scale stiffness of mouse aorta. Biophys J 2017;113:2540–51.

55. Dong L, Wijesinghe P, Dantuono J, Sampson D, Munro P, Kennedy B, et al. Quantitative compression optical coherence elastography as an inverse elasticity problem. IEEE J Sel Top Quantum Electron 2016;22. DOI: 10.1109/JSTQE.2015.2512597.
56. Dong L, Wijesinghe P, Sampson DD, Kennedy BF, Munro PR, Oberai AA. Volumetric quantitative optical coherence elastography with an iterative inversion method. Biomed Opt Express 2019;10:384–98.
57. Fang Q, Frewer L, Wijesinghe P, Allen WM, Chin L, Hamzah J, et al. Depth-encoded optical coherence elastography for simultaneous volumetric imaging of two tissue faces. Opt Lett 2017;42:1233–6.
58. Klein T, Huber R. High-speed OCT light sources and systems [Invited]. Biomed Opt Express 2017;8:828–59.
59. Fang Q, Krajancich B, Chin L, Zilkens R, Curatolo A, Frewer L, et al. Handheld probe for quantitative micro-elastography. Biomed Opt Express 2019;10:4034–49.